EUROPEAN ORGANIZATION FOR NUCLEAR RESEARCH
CERN — AB DEPARTMENT

CERN-AB-2006-013 ATB
EURISOL-DS/TASK2/TN-05-01

EURISOL-DS Multi-MW Target Preliminary Study of the Liquid Metal Proton-to-Neutron Converter

Adonai Herrera-Martínez, Yacine Kadi, and the EURISOL-DS Task#2 collaboration

Abstract

This technical note summarises the design calculations performed within Task #2 of the European Isotope Separation On-Line Radioactive Ion Beam Facility Design Study (EURISOL-DS) [1].

A preliminary study was carried out in order to determine the optimum value of relevant parameters in the target design. Different scenarios were simulated using the Monte Carlo code FLUKA [2]. Namely, sensitivity studies were performed to assess the impact of the projectile particle energy on the neutronics and energy deposition in the spallation target. The optimal target dimensions were also studied for every case as well as the proper target material for the liquid metal proton-to-neutron converter, since mercury and lead-bismuth eutectic are reasonable options. The effect of the beam width on the power densities was also evaluated, taking into account the geometrical limitations of the facility. Finally, a comparison between protons and deuterons as primary particles was performed, acknowledging the limitations of using FLUKA for these simulations.

The results of these calculations show the benefit of using protons as primary particles and increasing their energy, in order to reduce the high power densities occurring in the first few centimetres downstream from the interaction point. Particularly, a 2 GeV proton beam with a σ ~15 mm Gaussian distribution on a 15 cm radius 50 cm long target seems a suitable trade between increasing the neutron and fission yields and reducing the power densities in both, the liquid metal and fission targets.

Geneva, Switzerland
30 January, 2006

Table of Contents

Introduction

The production of neutrons through the spallation reaction is a well-known technique, studied since the 1950's and currently applied in a wide range of processes. It is based on a charged particle induced cascade in a generally high-Z and high-density material.

In such a charged particle induced cascade one can distinguish between two qualitatively different processes: a spallation-driven high-energy phase and a neutron-driven regime. In the first phase, neutrons are produced by spallation and act as a source for the following phase, in which they gradually loose energy by collisions and are multiplied, in some cases, by fission or (n, xn) reactions.

Therefore, depending on type of neutron source required (e.g. pulsed sources with a wide energy range for time-of-flight measurements, continuous sources presenting a hard spectrum for accelerator-driven systems etc.), one should choose carefully:

- The target material;
- The target dimensions;
- The incident particle type and energy.

Indeed, the choice of the target dimensions and material is a critical issue for the neutronics of the system and the operation of the facility. It has an impact in, for example, the activation of the facility or the neutron source efficiency. The nature of the incident particle is related to the spatial and energy distribution of the neutrons and the power densities in the target.

FLUKA: a general purpose Monte Carlo code

Fluktuierende Kaskade (FLUKA) is a general purpose tool for calculations of particle transport and interactions with matter, covering an extended range of applications spanning from proton and electron accelerator shielding to spallation target design, calorimetry, activation, dosimetry, detector design, Accelerator Driven Systems, cosmic rays, neutrino physics, radiotherapy etc. It can accurately simulate the interaction and propagation in matter of about 60 different particles, including neutrons down to thermal energies and heavy ions.

Below a few GeV, the FLUKA hadron-nucleon interaction models are based on resonance production and decay. Two models are used also in hadron-nucleus interactions: at momenta below 3-5 GeV/c the PEANUT package includes a very detailed Generalized Intra-Nuclear Cascade (GINC) and a preequilibrium stage, while at high energies the Gribov-Glauber multiple collision mechanism is included in a

less refined GINC. Both modules are followed by equilibrium processes: evaporation, fission, Fermi break-up, gamma deexcitation.

Moreover, an original treatment of multiple Coulomb scattering and of ionization fluctuations allows the code to handle accurately some challenging problems such as electron backscattering and energy deposition in thin layers even in the few keV energy range. For neutrons with energy lower than 20 MeV, FLUKA uses its own neutron cross-section library (P5 Legendre angular expansion, 72 neutron energy groups), containing more than 140 different materials. Neutron energy deposition is calculated by means of kerma factors; however, recoil protons and protons from (n, p) reactions are transported explicitly.

The EURISOL Project

The EURISOL DS [1] project aims at a design study of the 'next-generation' European Isotope Separation On-Line (ISOL) Radioactive Ion Beam (RIB) facility, which will extend and amplify, beyond the year 2010, the work presently being carried out at the first generation RIB facilities in Europe and other parts of the world, in the fields of Nuclear Physics, Nuclear Astrophysics and Fundamental Interactions.

The scientific case for high-intensity RIBs using the ISOL method includes (a) the study of atomic nuclei under extreme and so-far unexplored conditions of composition (i.e. as a function of the numbers of protons and neutrons, or the so-called isospin), rotational angular velocity (or spin), density and temperature; (b) the investigation of the nucleosynthesis of heavy elements in the Universe, an important part of Nuclear Astrophysics; (c) a study of the properties of the fundamental interactions which govern the properties of the Universe, and in particular of the violation of some of their symmetries; (d) potential applications of RIBs in Solid-State Physics and in Nuclear Medicine, for example, where completely new fields could be opened up by the availability of high-intensity RIBs produced by the ISOL method. These cases require a 'next generation' infrastructures such as the proposed EURISOL facility, with intensities several orders of magnitude higher than those presently available or planned, allowing the study of hitherto completely unexplored regions of the Chart of the Nuclei.

The main components of the proposed facility are: a driver accelerator, a target/ion-source assembly, and a mass-selection system. The driver accelerator investigated in this study is a 1–3 GeV, Multi-MW, superconducting proton linear accelerator, although the implications of enabling it to accelerate light nuclei was also considered. An alternative suggestion, i.e. an electron accelerator using brehmsstrahlung to

generate photofission, was also examined, but found to have limitations which would make it more expensive for the high yields demanded for EURISOL [3].

The proposed ISOL facility would use both (a) several 100 kW proton beams on a thick solid target to produce RIBs directly, and (b) a liquid metal 1–5 MW 'converter' target to release high fluxes of spallation neutrons which would then produce RIBs by fission in a secondary uranium carbide (UCx) target. An alternative windowless liquid mercury-jet 'converter' target to generate the neutrons has also been proposed for this Multi-MW target station.

This document deals with the design of such a Multi-MW target station, analysing the major parameters of the facility in order to optimise the production of the required isotopes through fission in the UCx target.

Parameters to Optimise

Since the purpose of the facility is to produce certain radioisotopes, maximising the **yield of such isotopes** is the main objective in the design. In the case of the proton-to-neutron converter this implies increasing the **neutron yield** and reducing the **parasitic absorptions** in the converter.

The **compactness and efficiency** of the spallation target is mandatory in order to minimise the total inventory of material in the facility and attain the specified **neutron flux** and **fission density**. Reducing the dimensions of the target would have a positive impact on the radioprotection and waste management of the facility (e.g. confinement of the radioactive material, lesser production of radioactive heavy metals to be disposed of) as well as it would cut the final costs of the project. Moreover, to increase the **fission rate** in a non-enriched target, the **neutron energy spectrum** should lay in the fast region, since fission cross-sections for non-fissile isotopes are higher at these energies. This harder neutron spectrum may be achieved by **decreasing the moderation** of the spallation neutrons in the target.

Last, but not least, minimising the **power densities** is a requirement in order to allow the evacuation of the heat from the converter, in particular from the liquid mercury target and the beam window interface. This is one of the most complicated issues when dealing with high power spallation targets.

Consequently, this preliminary study covers a broad range of parameters, which have to be optimised in order to propose some alternatives for the design. A non-comprehensive list of the parameters analysed is given below:

- Primary particle type: Protons and deuterons were considered;

- Primary particle energy: 1–3 GeV for protons and 100 MeV–1 GeV for deuterons;
- Target dimensions: radii ranging from 10 to 40 cm and active lengths ranging from 40 to 100 cm were studied;
- Target material: mercury was compared to lead bismuth eutectic as target material in terms of neutron production and power densities;
- Beam profile: the optimum beam standard distribution was studied in order to decrease the power densities.

Model Layout

Initially, the beam particles considered were protons with an energy of 1, 2 or 3 GeV, following a Gaussian distribution with a standard deviation of 1.7 mm in both x and y directions. The dimension of the target varied from 40 to 100 cm in length and 10 to 40 cm in radius. Figure 1 illustrates an artistic view of a 60 cm, long 20 cm radius target, with a 20 cm long, 2 cm radius vacuum along the proton line in order to reduce the possible particle backscattering through the front cap.

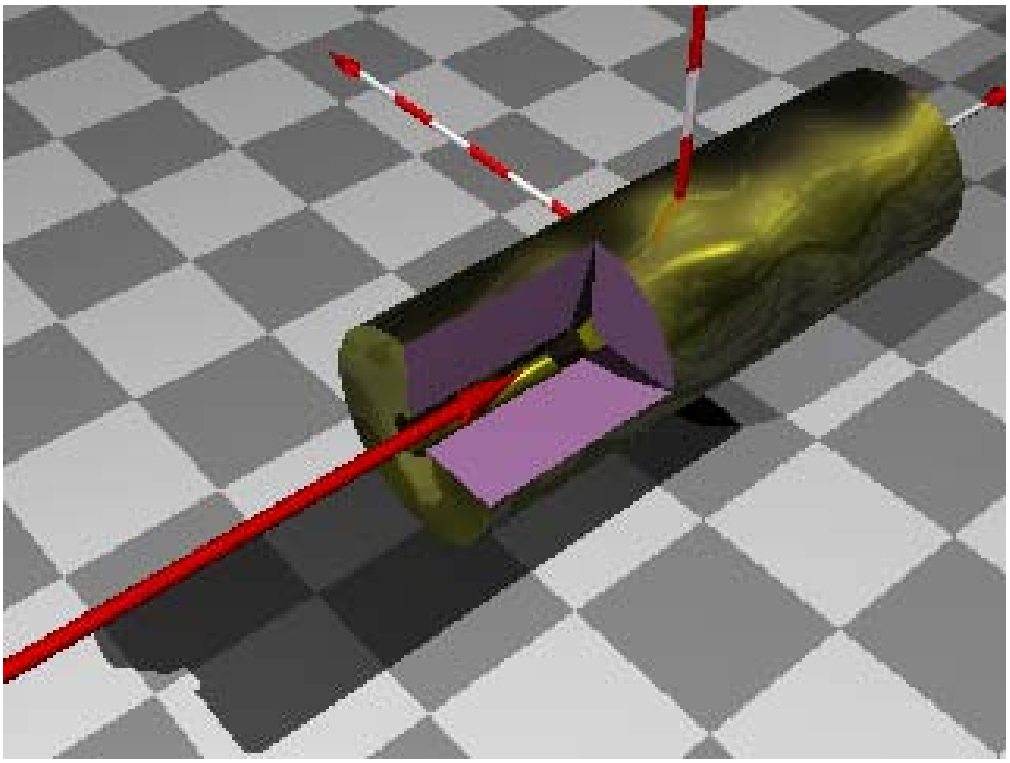

Figure 1. 3-D view of the Multi-MW EURISOL target.

Proton Energy

The energy of the incident particle is strongly related to the maximum distance these particles can reach hence to the dimension of the target to maintain below a certain limit the number of charged particles escaping. For the energy range considered (1–3 GeV) the proton range in Hg increases greatly, going from ~46 cm for 1 GeV, to ~110 cm for 2 GeV and ~175 cm for 3 GeV protons.

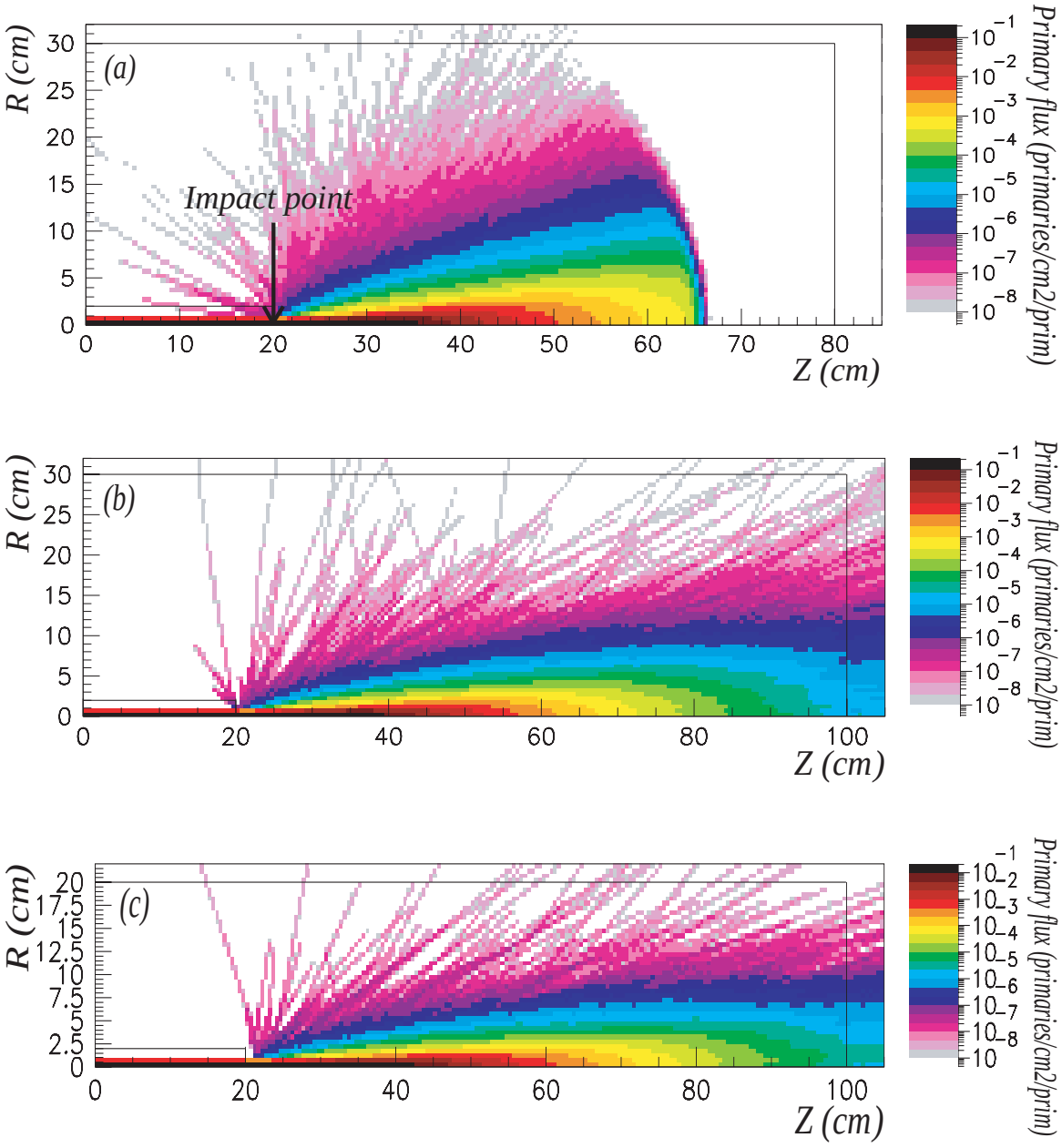

Figure 2. Primary particle distribution (particles/cm^2/primary) for different incident proton energies: (a) 1 GeV, (b) 2 GeV, (c) 3 GeV, and Hg target dimensions.

Figure 2 shows the primary proton distribution after impacting on a Hg target and the beam impact point, 20 cm from the origin of the model, for the different proton energies analysed. In the case of 1 GeV protons (a), an 80 cm long 30 cm radius fully contains the beam, whereas for 2 GeV (b) and 3 GeV (c) even a 100 cm long (80 cm active length) target prevents some primary protons from escaping. For the 2 GeV case, the level of these escapes is ~2×10^{-5} primary escapes/cm^2/primary through the end cap surface, whereas for the 3 GeV case it increases up to ~5×10^{-5} primary escapes/cm^2/primary, with an average energy of ~750 MeV, thus still capable of producing spallation and high-energy fissions in the structures downstream.

For 1 GeV protons, the primary shower (down to 10^{-6} primaries/cm^2/primary) is contained within a solid angle of ~20 degrees. For 2 and 3 GeV, the shower is more forward –peaked, being contained within ~10 and ~8 degrees respectively, therefore allowing a reduction of the target radius to about 10–15 cm, as far as the primary escapes are concerned. Few primary backscattering occurs for 1 GeV protons, but disappear totally at higher energies, thus reducing the need of a beam vacuum inside the target.

Neutron Spatial Distribution

The neutron yield increases with the incident proton energy and with the volume of the target (decreasing escapes). Nevertheless, the slope of this tendency changes both with the target length and radius. Figures 3.(a), (b) and (c) illustrate this evolution for 1, 2 and 3 GeV, respectively. It can also be seen that, for every energy, there are some target dimensions beyond which the efficiency of the source does not increase significantly.

Namely, for 1 GeV protons, any dimension beyond the proton range has a minor contribution to the neutron yield. For example, an increase in the target radius from 10 to 20 cm increases the yield by 20 %, whereas going from 30 to 40 cm radius adds only a 3 % to the neutron yield. For the target length and 2 GeV protons, extending the target from 60 to 80 cm would increase the yield by ~18%, whereas an increase from 80 to 100 cm would just augment the yield by ~4%.

Moreover, as it will be explained later, an excessive increase in the target dimensions actually decreases the overall neutron population due to the neutron captures in the periphery. These results conclude that a 20–30 cm radius and a 60 cm (for 1 GeV) or 80 cm long (for 2 and 3 GeV) target is enough for an efficient production of neutrons.

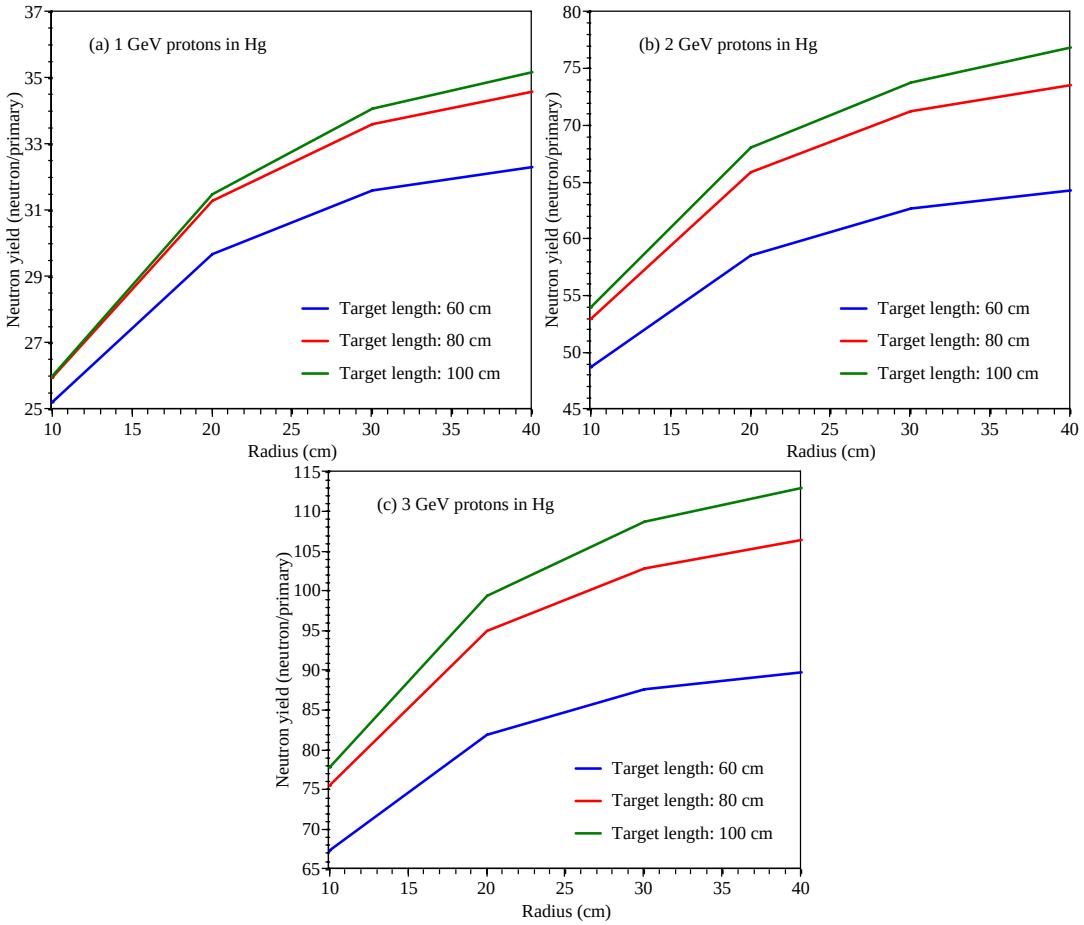

Figure 3. Neutron yields (neutrons/primary) as a function of the target dimensions for (a) 1 GeV, (b) 2 GeV, (c) 3 GeV incident proton energy.

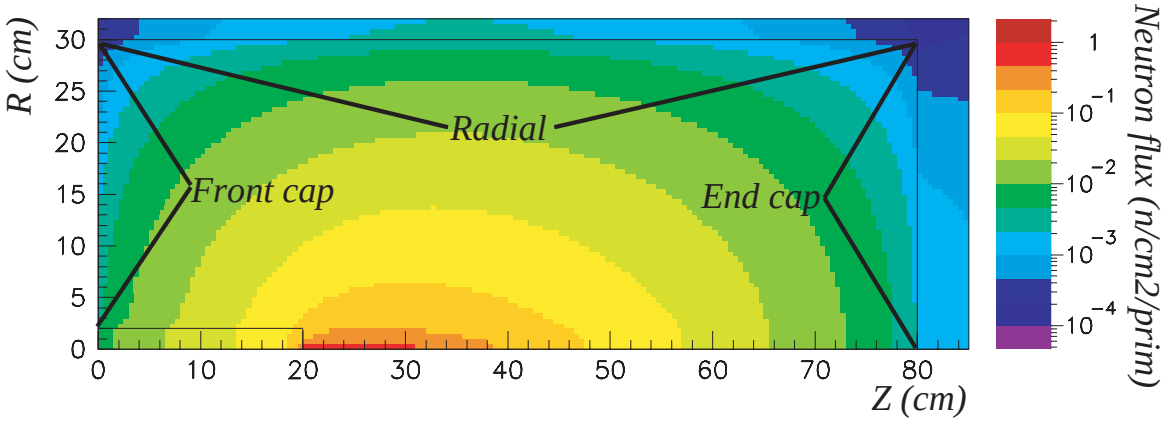

Figure 4. Neutron flux (neutrons/cm^2/primary) distribution for a 1 GeV proton beam.

Figure 4 shows the neutron flux distribution for 1 GeV primary protons. The flux is centred radially around ~10 cm from the impact region (30 cm along the Z-axis in Figure 4). It becomes isotropic beyond 15 cm from this centre point, and, since the

flux presents a spherical distribution, it decreases with the square of the distance to its centre.

The neutron flux for 2 and 3 GeV follows a similar distribution to the one for 1 GeV, with the exception of a shift in the centre of the spherical distribution, which lies at ~15 cm from the impact point for 2 GeV protons and at ~20 cm for 3 GeV protons. For these higher energies, the high-energy component (above 20 MeV) in the neutron flux gains weight, as explained later in the analysis of the neutron energy distribution.

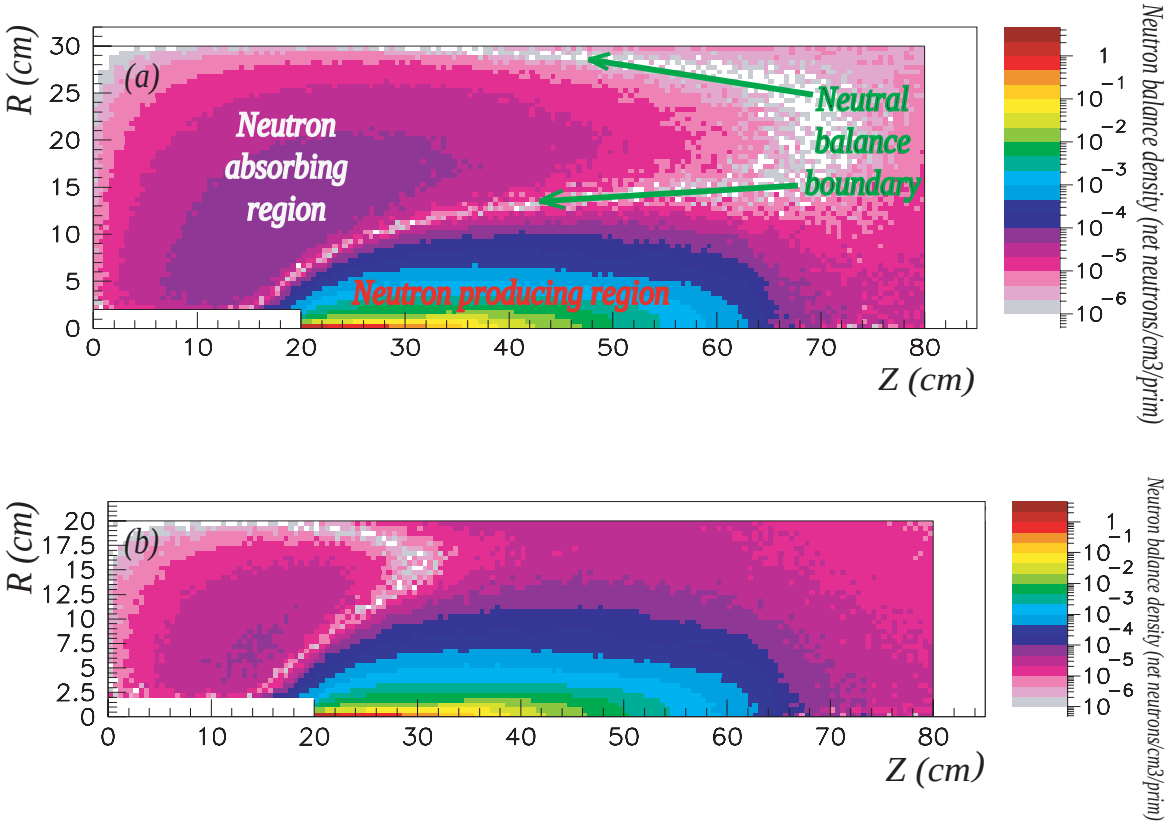

Figure 5. Neutron balance density (in absolute values, net neutrons/cm^3/primary) in Hg for a 1 GeV proton beam for a 30 cm radius 80 cm long target (a), and a 20 cm radius 80 cm long target (b).

As far as the neutron balance density (algebraic sum of neutrons produced minus neutrons captured) is concerned, the neutron-producing region follows the primary particle distribution. For 1 GeV protons (Figure 5), neutrons are mainly produced up to 10 cm upstream from the interaction point. The neutron-producing region extends to the end of the target, although the regions beyond the proton range present a very small contribution (~10 ppm) to the total neutron balance. Most of the neutron population is produced within a radius of 12 cm.

The behaviour for 2 and 3 GeV primaries is very similar except for an axial increase of the neutron-producing region (bound to the evolution of the primary flux); radially,

the distribution does not change with primary energy. Finally, the region around the beam line vacuum (from Z 0 to 20 cm in Figure 5) absorbs more neutrons when the primary energy is increased; this is due to the fact that the spallation neutrons are produced farther away from the interaction point with increasing primary energy and therefore, these secondary neutrons undergo a larger number of scattering reactions, reaching the aforementioned region at lower energies.

Hence, the region beyond a 10–12 cm radius represents a minor contribution to the total neutron balance and even acts as an absorbing region, as shown by Figure 5.(a) and (b). Any length beyond the proton range is not necessary (even the last portion of the range) and the region upstream from the impact point should be reduced to about 5 cm and reshaped according to the positive neutron balance distribution.

Neutron Energy Distribution

The neutron energy distribution is a relevant issue, since the fissionable material, i.e. U-238, presents a threshold fission cross-section, for which practically no fissions are produced below the MeV region. Therefore, a hard neutron spectrum should be favoured and balanced against an acceptable containment of the charged particles.

In this sense, figures 6.(a), (b), (c) and (d) illustrate the energy distribution of the spallation neutrons per MW of beam power (a) inside the target, (b) escaping downstream, (c) escaping radially and (d) backscattered through the front surface, for 1, 2 and 3 GeV primary protons and a 20 cm radius 80 cm long Hg target.

In all these figures, the escaping neutron spectrum is dominated by evaporation neutrons having undergone some moderation (peak at ~300 keV), since normally their distribution peaks at 2–3 MeV; there is also a significant component of neutrons with energies greater than 100 MeV, especially in the forward direction, due to direct knock-out interactions between the primary protons and single nucleons (intra nuclear cascade).

The normalised neutron energy spectra seem quite similar for all three incident proton energies, except for the neutrons escaping through the end cap (at 60 cm from the impact point, Figure 6.(d)). In that area, the neutron flux increases with the energy due to the extension of the neutron-producing region and the longer range of the high-energy particles (in the case of 1 GeV incident protons there is a reflection effect for the volume beyond the range).

The neutron flux through the radial surface of the target is several times larger than the one through the front cap or the end cap. Nevertheless, the neutrons crossing the end cap surface present a more significant high-energy region (above 10 MeV),

making the neutron spectrum through that source harder, thus more likely to produce high-energy fissions in U-238.

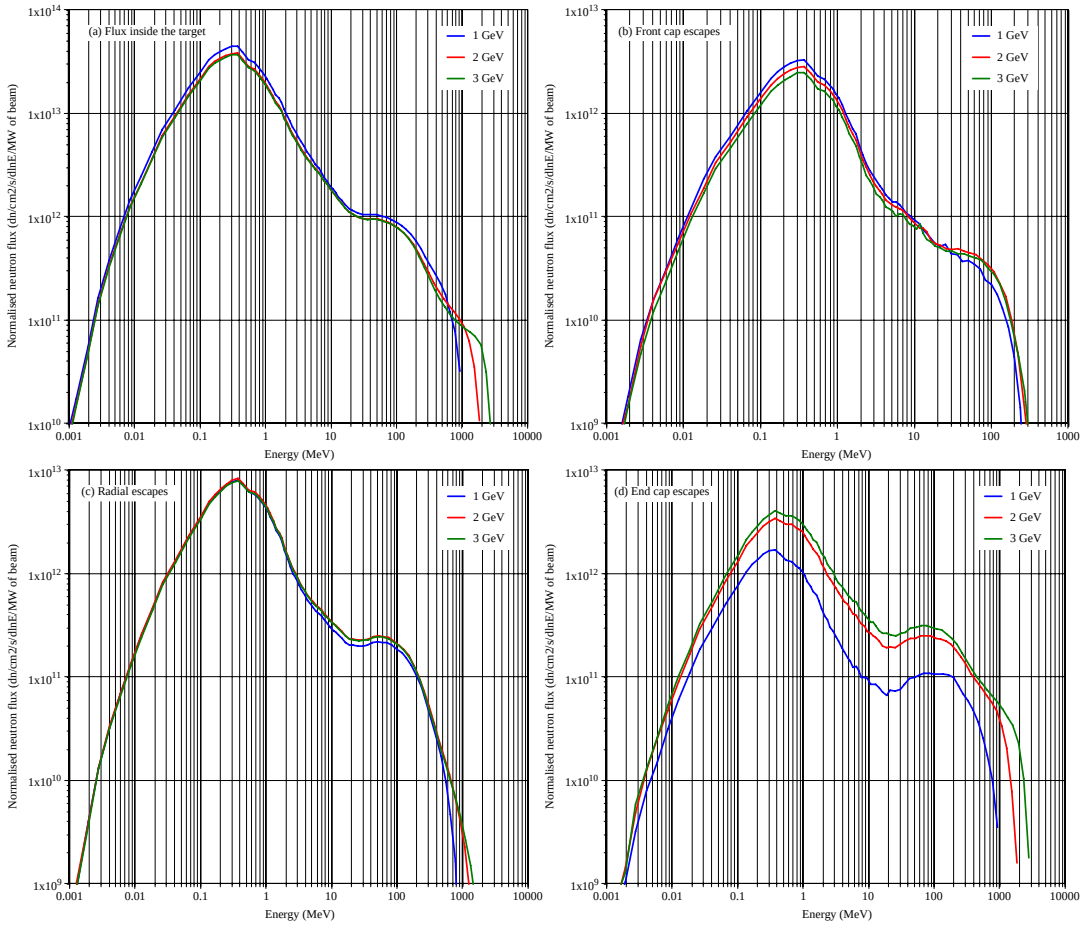

Figure 6. Neutron energy spectrum (neutrons/cm^2/s/dlnE/MW of beam) for different positions of the 20 cm radius 80 cm long Hg target.

As indicated previously, the fission cross-section of U-238 below 2 MeV is rather low (~10^{-4} barn in the ENDF/B-VI.6 nuclear data library, Figure 7.(a)), increasing to ~1.7 barns at 35 MeV (Figure 7.(b) [4]). The alternative use of natural uranium (99.3% wt. U-238 and 0.7% wt. U-235) should be considered since U-235 presents a significantly higher fission cross-section from thermal to fast energies (up to 20 MeV). The one-group fission cross-section of natural uranium for an unreflected neutron flux, such as the one escaping the Hg target radially (Figure 6.(c)) is ~0.097 barn, compared to the ~0.087 barn of U-238 (or the ~1.395 barn of U-235). Although the gain in fission rate by using natural uranium instead of pure U-238 is rather small (i.e. 11%), in the case of a reflected system where the escaping neutrons are bounced back by the reflector at a lower energy, the effect of the small U-235 fraction in natural uranium may be significant.

On these premises, there may be several geometrical configurations for the fissile target (most probably, UCx). A first approach may be to place the fissile material around the target, in order to use the maximum number of neutrons (higher fluxes) to produce fission (Figure 8.(a)).

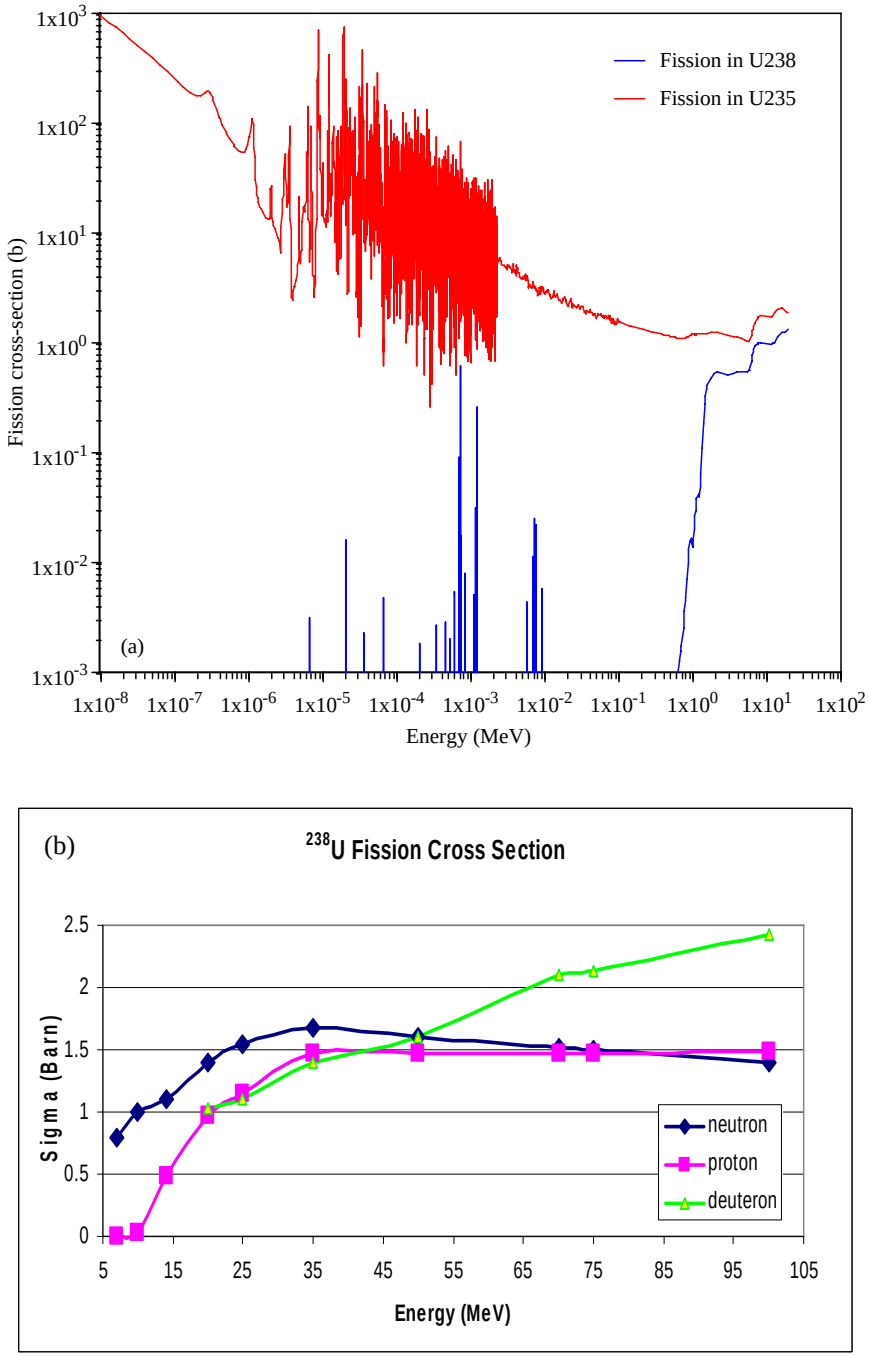

Figure 7. Comparison of the U-235 and U-238 fission cross-sections from ENDF/B-VI.6, and the U-238 fission cross-section above 5 MeV for different projectiles [4].

Another option is to shorten the converter, accepting a certain level of energetic charged particles into the fissile target, and placing the target in front of the converter

(Figure 8.(b)). This last solution presents obvious technical advantages, such as the complete decoupling of the UCx target from the mercury target. On the other hand, and as it will be demonstrated latter, to maximise the efficiency of the neutron-to-proton converter and increase the absolute fission rates, the fissile target should also be placed around the spallation neutron source.

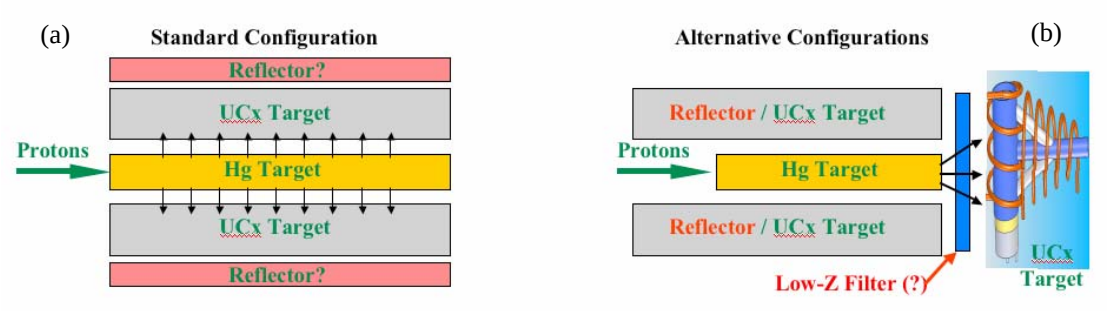

Figure 8. Possible configurations for the proton-to-neutron converter coupled to the fission target.

Target Material: Mercury vs Lead-Bismuth Eutectic

Although mercury is the proposed material to act as proton-to-neutron converter, due to its high neutron yields and convenient thermo-mechanical properties (liquid at ambient temperature and high density), other target materials are possible. In particular, the use of lead-bismuth eutectic (henceforth referred to as LBE) should be studied due to its, arguably, more favourable neutronic properties.

The incident proton distributions are rather similar for both materials, except for the proton range: ~46 cm in Hg for 1 GeV incident energy compared to ~60 cm in LBE (30% longer, due to the 30% increase in density from LBE to Hg).

A similar situation results in the overall neutron flux distribution, where the shape of the distribution is the same, but higher values of neutron flux appear in the periphery of the target. As explained later, this is due to the lower LBE capture cross-section compared to Hg.

The most significant discrepancy is obtained by analysing the neutron balance densities (Figures 9.(a) and (b)), which present a net neutron absorbing region in Hg for a radius greater than 12 cm and a length greater than 70 cm, whereas the whole target volume has a positive neutron balance when LBE is used. In other words, no parasitic captures occur in the LBE target.

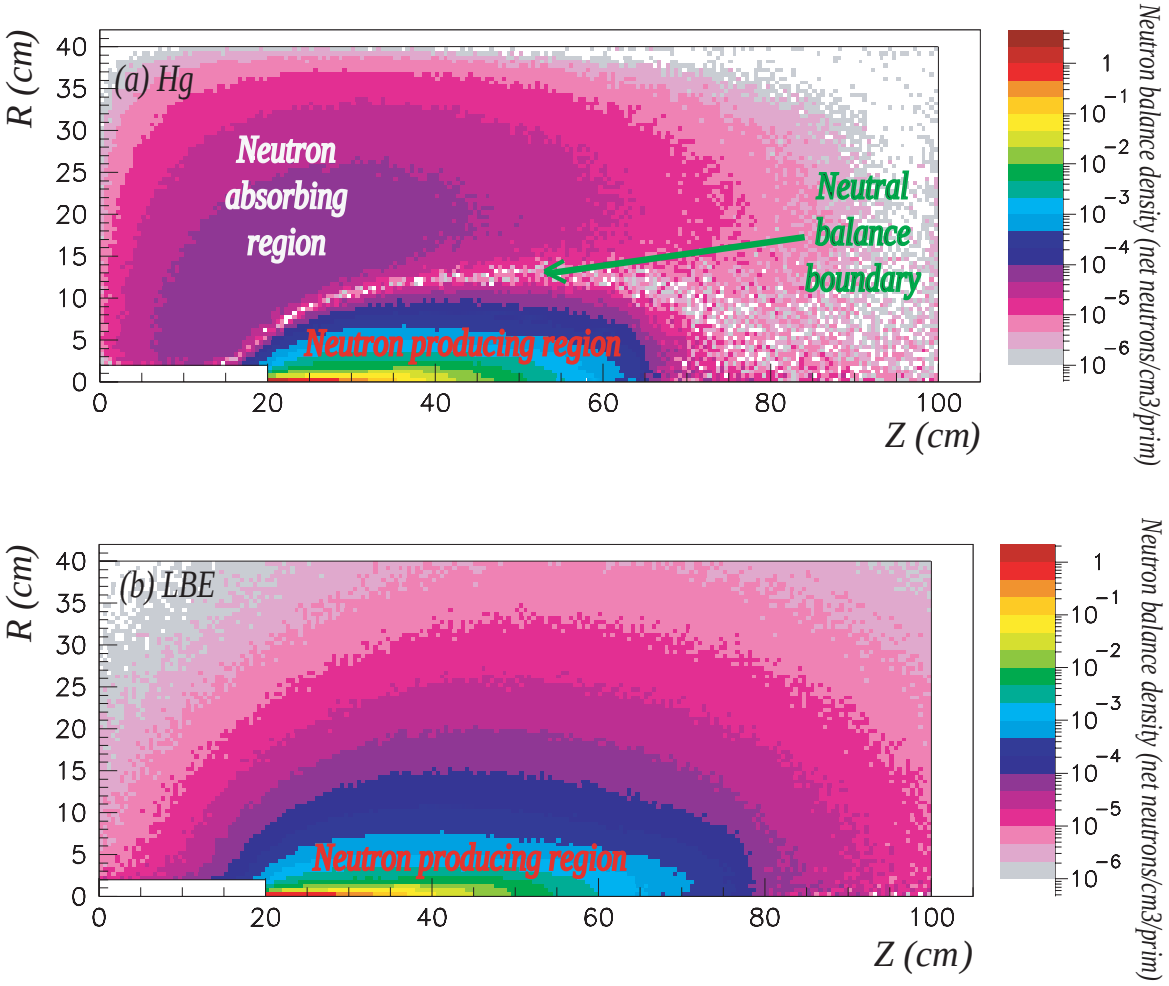

Figure 9. Neutron balance densities for 1 GeV incident protons in a 100 cm long 40 cm radius (a) Hg, (b) LBE, targets.

This improvement in the neutron efficiency is due to the significantly lower capture cross-sections of the isotopes forming LBE (i.e. Bi-209 and Pb-204, 206, 207, 208) compared to those forming natural Hg (i.e. Hg-196, 198, 199, 200, 201, 202, 204), as exemplified by Figure 10, where the total and capture cross-sections of natural Hg and LBE used by FLUKA (using 72 neutron energy groups between thermal energies and 19.6 MeV) are represented.

In the case of LBE, the total cross-section is rather flat, in particular below the keV region. This is due to the dominance of elastic scattering over the other reactions. On the other hand, for Hg and that energy range the total cross-section decreases with $1/\sqrt{E}$, since it is dominated by capture. This implies that the neutron flux below the keV region in LBE will be significantly higher than in Hg due to the reduced number of captures. Above 100 keV, the total cross-sections of both materials are quite similar.

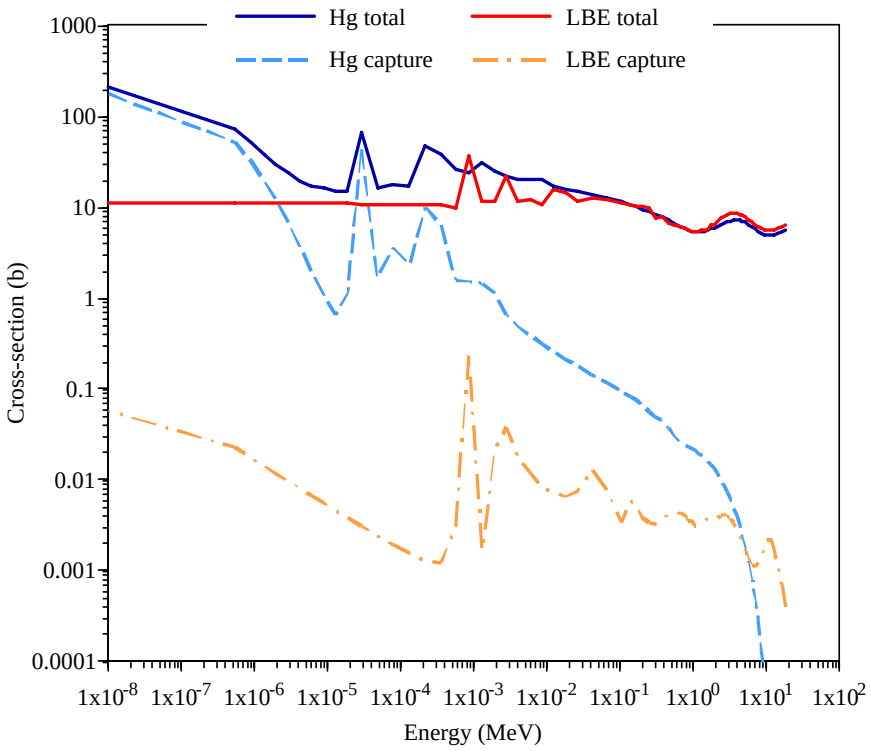

Figure 10. Comparison of the total and capture neutron cross-sections of LBE (from ENDF/B-VI.6) and Hg (from (JENDL-3.3), used by FLUKA.

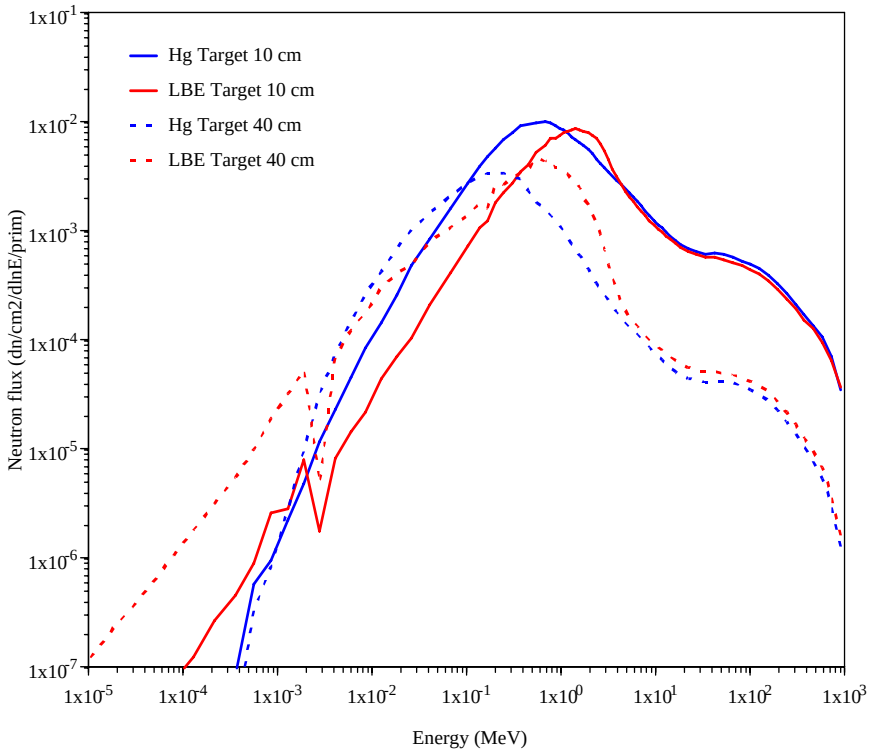

Figure 11. Neutron energy spectrum inside the target volume, for Hg and PbBi, and 10 cm and 40 cm targets.

These differences in the cross-sections have a more direct implication in the neutron energy spectrum inside the target, as shown in Figure 11. For a 10 cm radius target, the differences between Hg and LBE start below 3 MeV. In this energy range, LBE presents a slightly harder spectrum, peaking at ~1.3 MeV, whereas the spectrum using Hg peaks at ~600 keV. For intermediate energies (from MeV to keV) the flux in Hg is higher due to its higher efficiency in containing the primary shower (through neutron-producing reactions).

For low energies (below a few keV), the higher capture cross-section of Hg plays a significant role in cutting down the flux, hence its use for pulsed neutron sources (i.e. SNS), where the separation between bunches is enhanced by the capture of moderated neutrons from the previous pulse. In general, for a 10 cm target, Hg seems more efficient, producing a total neutron yield of 19.1 neutrons per incident 1 GeV proton, in contrast with the 15.5 neutrons per proton produced in LBE.

On the other hand, for a target where the primaries are fully contained (e.g. 1 GeV protons on a 40 cm radius 100 cm long target), the differences become significant. The neutron flux presents a higher value for LBE in almost the whole energy range, peaking at ~700 keV, while for Hg it reaches its highest value at ~200 keV. The neutron yields are rather similar (34.1 and 35.3 neutrons per primary proton for LBE and Hg, respectively) but the integral neutron flux is significantly larger, due the higher importance of the epithermal neutrons (due to an enhanced moderation), as exemplified by figures 10 and 11.

As previously elaborated, if high-energy reactions are to be prioritised (i.e. fission in U-238), a smaller target (10–15 cm radius) seems more convenient to obtain a harder spectrum, despite the poorer neutron yields and low energy neutron flux. In this sense, the use of LBE does not present a clear advantage. Moreover, LBE presents a higher level of activation when compared to Hg, mainly due to Po production by neutron capture in Bi, which would increase the complexity of the radioprotection and waste management of the facility.

Concerning power densities, LBE presents a maximum of ~21 kW/cm^3/MW of beam for 1 GeV protons, 22% lower than the ~27 kW/cm^3/MW of beam in Hg. Nevertheless, the differences in the thermo-mechanical properties of both materials, as presented in Table 1, may have an impact in the temperature reached by the liquid metal. Therefore, a precise thermal analysis of the flow should be performed for a detailed model to define the cooling strategy for either one of the liquid metal targets.

Another issue may be the production of radiotoxic volatiles in the target due to the spallation reactions and activation. This subject should also be addressed in detail,

since it could have great importance in the waste treatment of the target while in operation, as well as, once the target is to be disposed.

Table 1. Several mechanical and thermal properties of the proposed target materials [5].

Target Material	Density (g/cm^3)	Specific heat (J/g/K)	Melting temperature (°C)	Boiling temperature (°C)
Mercury (Hg)	13.546	0.139	-38.83	356.73
Lead-bismuth eutectic (LBE)	10.5	0.15	125	1560 (Bi) 1740 (Pb)

As a conclusion, a small (~15 cm radius) Hg target presents clear advantages in the containment of the primary particles and the efficiency of the neutron source, although its low boiling point (~357 °C) makes the heat removal a priority in the design of a high-power spallation source. For a larger target, LBE should be considered, principally due to its better neutron economy (lower capture cross-section) and higher boiling temperature, albeit the possible production of more radiotoxic species (such as Po and the volatile Hg-196, for instance).

Energy Deposition

A critical issue for the design of a high-power spallation source is the precise definition of the energy deposition in the different elements of the target. As a matter of comparison, the difficulties undergone to design the target cooling for the Spallation Neutron Source (SNS), a 1.4 MW (1.4 mA @ 1 GeV) beam on Hg, are well known. The EURISOL Multi-MW target is planned to sustain a 4–5 MW beam, thus, a priori, withstanding more extreme working conditions than the former.

In these preliminary calculations using a quasi pencil-like beam ($\sigma_{x,y}$~1.7 mm), the interest is particularly set on the difference in power densities as a function of the densities, not in the absolute values, which would produce very large temperature increases.

For 1 GeV protons, the largest energy deposition occurs in the first 14 cm after the impact point, along the beam axis, as illustrated by Figure 12, with a maximum value of ~27 kW/cm^3/MW of beam power at ~0.8 cm from the impact point. Once the proton range is reached, the power densities drop sharply, to values below 5 W/cm^3/MW of beam. Large deposition gradients appear radially in the interaction region due to the narrow beam shape.

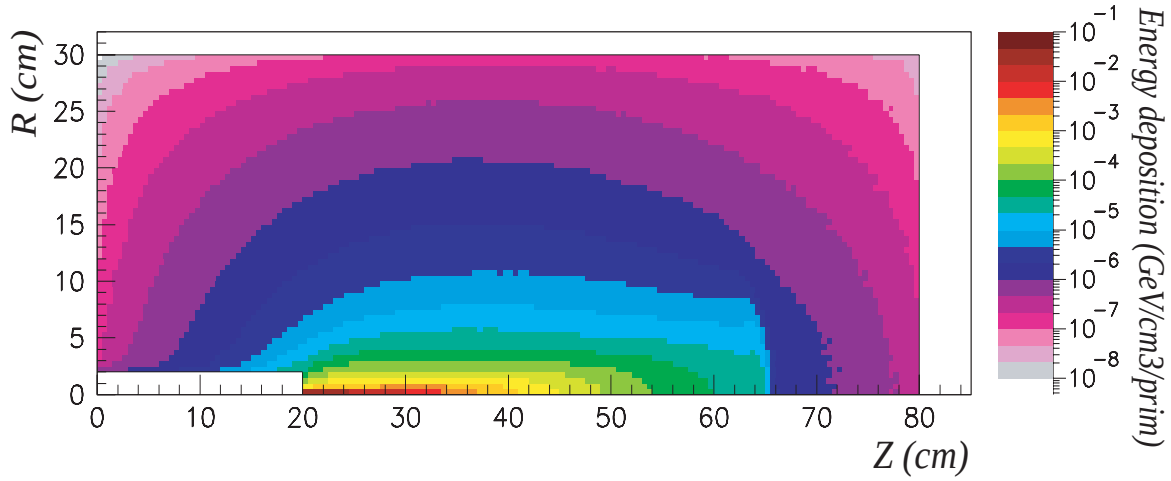

Figure 12. Energy densities (GeV/cm^3/primary) in a Hg target for a 1 GeV proton beam.

For 2 and 3 GeV primaries, the distribution of the energy deposition in the target is similar to that of 1 GeV protons, except for the region presenting the largest power densities, which extends considerably more in the axial direction. For 2 GeV protons, the maximum, ~16 kW/cm^3/MW of beam power (41% lower than that of 1 GeV protons), occurs at 1.2 cm from the impact point. For 3 GeV protons, the maximum power density is ~12 kW/cm^3/MW of beam power (56% lower than in the case of 1 GeV protons), taking place at ~1.4 cm from the beam impact point.

These results indicate that increasing the beam energy, e.g. to use 2 GeV primaries, may be essential in reducing the maximum power densities, thus easing the thermo-hydraulic problems related to heat evacuation from the target. However, another parameter can be optimised in order to achieve the same goal, as elaborated in the following section.

Impact of the Beam Profile

For a fixed beam power, the size of the Gaussian beam is quite relevant to the maximum power densities occurring in a spallation target. In order to assess the precise impact of the beam standard deviation (σ), several calculations were performed in the aforementioned 20 cm radius 80 cm long target and with 1 GeV incident protons, varying the value of σ_x and σ_y from 1.7 mm to 2, 5, 10, 15, 20, 25 and 30 mm. The results (normalised to 1 MW of beam power) are shown in Figure 13.(a), where an exponential (with negative exponent, of course) tendency can be perceived.

In order to properly contain the beam, the beam pipe should have a radius of approximately 3σ (99.7% of the beam particles contained inside). Moreover, the

proton-to-neutron converter itself should contain the beam in order to maximise its efficiency, therefore a trade between beam size and target size should be made. A beam size of σ ~15 mm seems appropriate to reduce the maximum power density from ~27 kW/cm^3/MW of beam to ~1.8 kW/cm^3/MW of beam power (15 times less). A further increase in the beam size may also be foreseen (for example going from σ ~15 mm to 25 mm reduces the maximum energy deposition by a factor of 2.4), although the dimensional requirements may impose some constraints, and the attained reductions in the power densities are smaller.

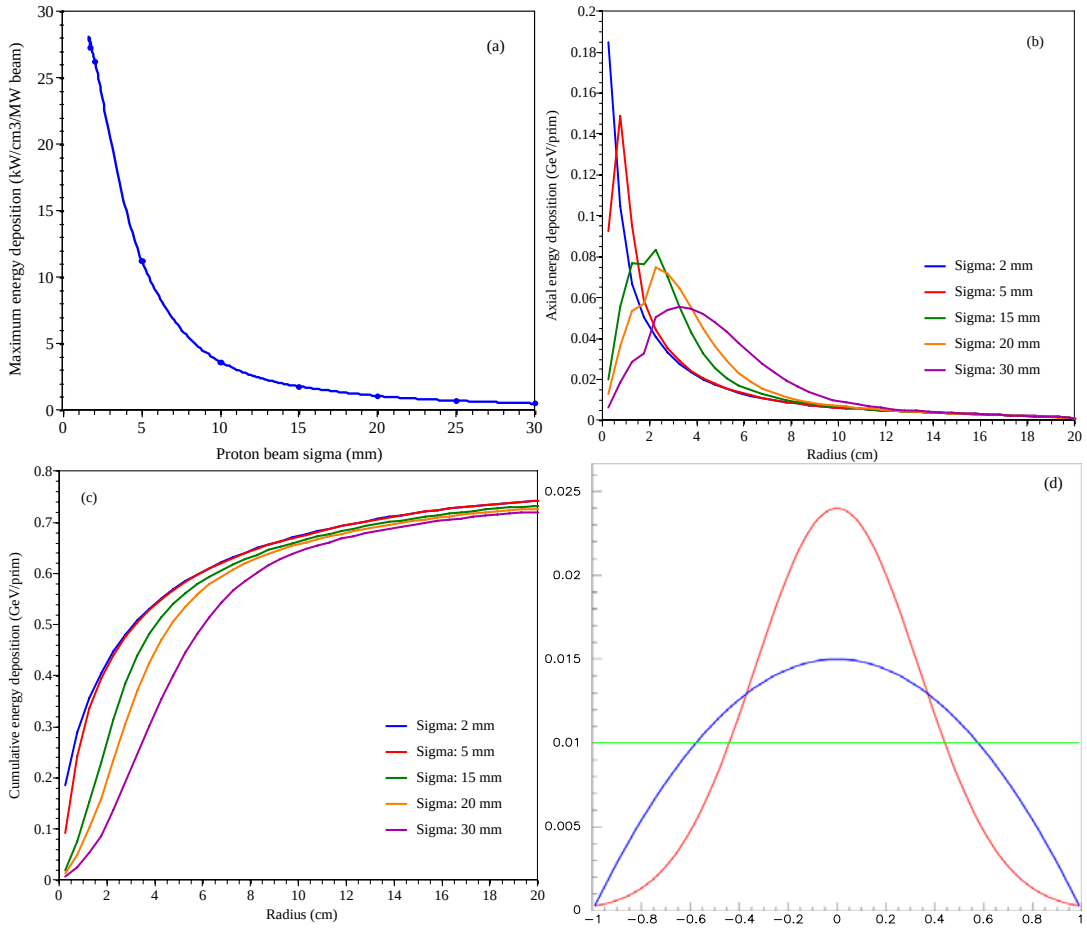

Figure 13. Evolution of the energy deposition as a function of the beam shape: (a) maximum power density as a function of σ; (b) sum of the energy deposited along z, as a function of the radius of the target, for different σ; (c) integral over the radius of the previous plot; (d) differences in the beam distribution for a flat, parabolic and Gaussian beam, for the same integral value (i.e. same intensity).

Figure 13.(b) presents the axial energy deposition as a function of the radius, that is, the sum of the energies deposited along the target axis for a certain radius. One can see that for smaller σ, i.e., 2 mm and 5 mm, most of the energy is deposited along the beam axis or at small radii, whereas for larger σ, i.e. 20 mm or 30 mm, most of the energy deposited is **spread** over a larger volume (e.g. for σ = 30 mm, the maximum

value is reached at 3.5 cm from the axis), therefore, reducing the maximum power densities. Figure 13.(c) is obtained taking the sum of the previous curve (b) for increasing radii. This figure suggests that, in this range of σ's, ~75% of the beam energy is deposited inside the target, independent of the beam width. In other words, σ has only an impact on the energy deposition for small radii and thus for reduced fractions of the beam energy contained.

Apart from altering the beam width, changing its shape may also reduce the power densities. Gaussian distributions tend to have very mid value decreasing quickly with the distance from the centre. An alternative would be to use a parabolic beam, which just by simple geometry (and normalising to the same area, in our case same current) presents a 40% lower maximum value. Figure 13.(d) exemplify this fact, where a Gaussian distribution of 3σ between –1 and 1 (thus, only 0.3% of the beam is collimated) is compared with a parabolic distribution and a flat distribution (in theory, the optimum), all of them normalised to the same area. Consequently, a parabolic beam of at least 4.5 cm radius would be strongly proposed.

Projectile Particle: Proton vs Deuteron

To determine the optimum primary particle to use, a comparison between deuterons and protons was also carried out using FLUKA. It should be noticed that this Monte Carlo code presents relevant limitations in simulating the deuteron interaction with matter. While the deuteron nuclear interactions are properly evaluated in this code and the total cross-section is in agreement with experimental data, the deuteron splitting reaction (comprising Coulomb and hadronic dissociations) is not accounted for. This reaction is particularly relevant for deuterons, since its threshold energy is only 2.2 MeV (compared, for example, to the 8 MeV for tritium or 14 MeV for He-4).

Therefore, in order to evaluate the error implicit in these calculations, the results of the FLUKA simulations using deuterons are compared with the results obtained by simulating the initially split deuteron, i.e. independently transporting a proton and a neutron, both with half the kinetic energy, and adding the results. This comparison suggests the limits of the error due to the lack of the splitting process in the code.

In order to give a rough idea of the relevant the deuteron dissociation in the overall non-elastic cross-section, Figure 14 shows the Coulomb dissociation cross-section [6] as a function of the deuteron energy for different isotopes (a), which gains importance for high-Z elements, and the total non-elastic cross-section for deuterons in natural lead used by FLUKA. As illustrated by Figure 14.(a), the Coulomb dissociation cross-section decreases with increasing energy, to a constant value of about 180 mb above

600 MeV, for Hg-202. Therefore, the Coulomb dissociation accounts for ~16% of the high-energy reactions of deuterons in Hg. The hadronic and Coulomb dissociations are estimated to be in the same range of values; hence their combined effect may be relevant in the simulation of deuterons at these energies.

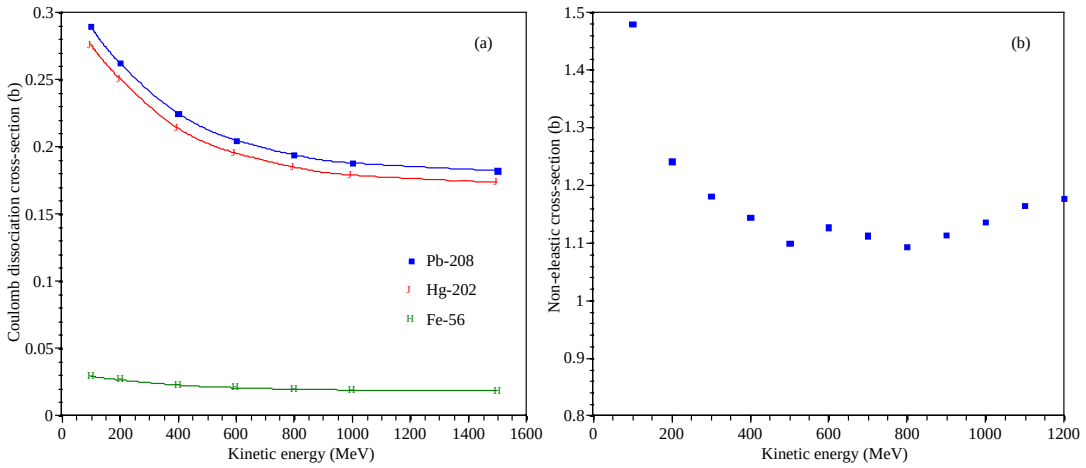

Figure 14. Deuteron cross-section for (a) Coulomb dissociation in different materials [6], (b) non-elastic reactions in natural Pb.

Under these premises, the comparison of the neutron yields between protons and deuterons is presented in Figure 15.(a), as function of the projectile's energy. Deuterons and protons, in general present similar yields, with higher neutron production when deuterons are used (~15% higher for 1 GeV). The breakeven point (protons and deuterons present the same neutron yield) for high-Z elements occurs at around 500 MeV, at higher energies than for low-Z targets. The efficiency of the neutron yields (as the ratio between the yield and the incident particle energy) also increases with energy for protons and deuterons, as illustrated in Figure 15.(b).

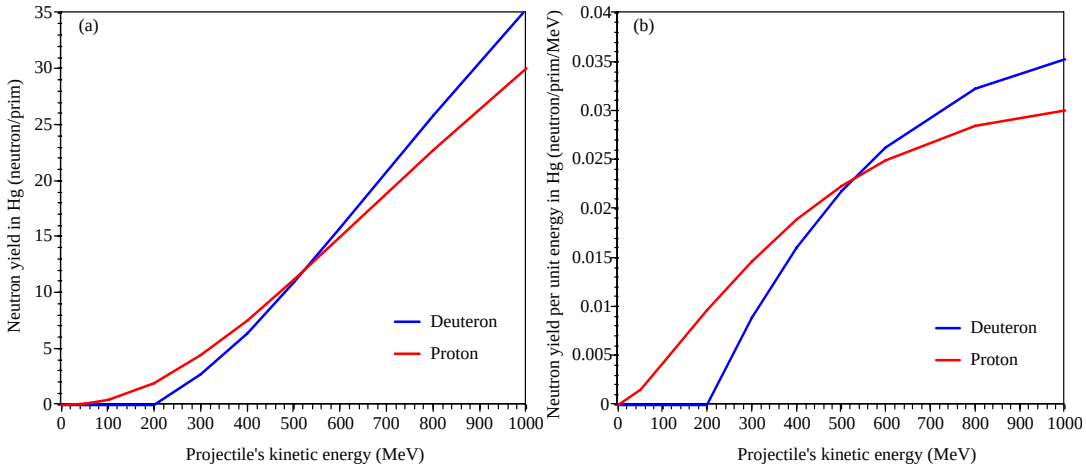

Figure 15. Neutron yield in Hg for different types of projectile.

Concerning the neutron flux distributions, Figure 16.(a) shows how this parameter evolves along the central axis of the target for different incident energies. The point of highest neutron flux is barely displaced with increasing projectile energy. On the other hand, the neutron production is distributed along a longer distance for higher energies, producing a larger integral neutron flux (normalised per MW of beam power and a Gaussian beam distribution of σ ~1.7 mm). Thus, higher energy particles, either deuterons or protons, produce higher and more evenly distributed neutron fluxes, similar to what occur with the energy deposition, as will be shown later in the section.

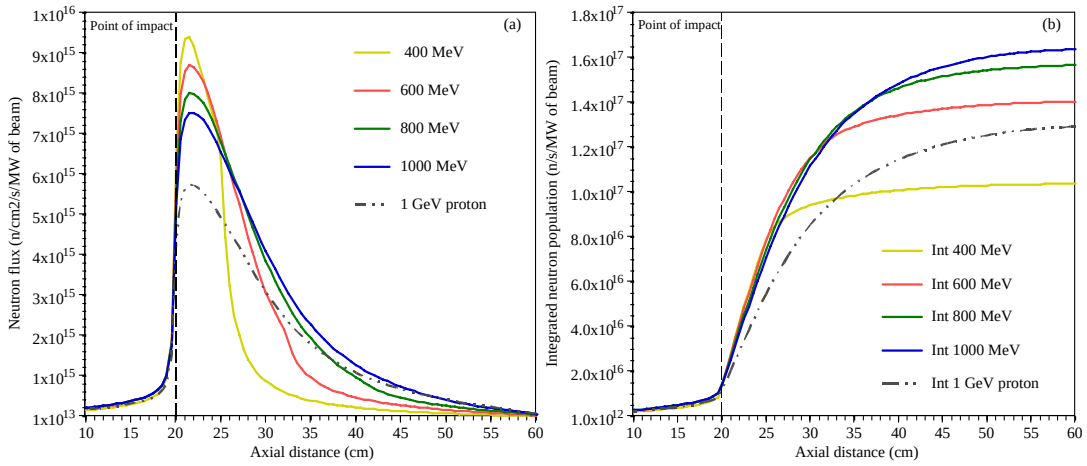

Figure 16. Neutron flux along the beam axis (a); sum of the neutron population along the beam axis, for an increasing distance from the impact point.

Nevertheless, most of the secondary neutrons are produced in the first 20 cm along the beam axis from the interaction point (Figure 16.(b)), entailing a relatively short active length, compared to the total length of the target (mainly required to reduce the primary flux through the end cap).

The evolution of the neutron energy spectrum along the target for different energies is, as discussed previously, an important factor in order to maximise the high-energy fissions. Due to the deuteron splitting limitations, spectra below 400 MeV are not reliable, given that very few neutrons are produced per incident deuteron. In fact, for energies below 800 MeV, the results between the deuteron with dissociation and the split deuteron (neutron and proton separately) differ significantly (Figures 17 (a) and (b)). Conversely, for higher energies, i.e. 800–1000 MeV, the discrepancies disappear gradually, except for the very high energy neutrons produced by an early dissociation, carrying half the kinetic energy of the projectile, which would escape the end cap at very small angles (strongly forward peaked). Below this range in the spectrum, 800 and 1000 MeV deuterons and protons present a very similar neutron energy distribution, in the middle of the target, radially and through the end cap.

For lower energies, the use of deuterons as a projectile particle may bring about a higher and harder neutron spectrum, in particular along the beam axis. On the contrary, for higher energies, such as the ones proposed for the Multi-MW target, namely 1000 MeV, the differences are rather small, not evidencing clearly the advantage of using deuterons as projectile instead of protons.

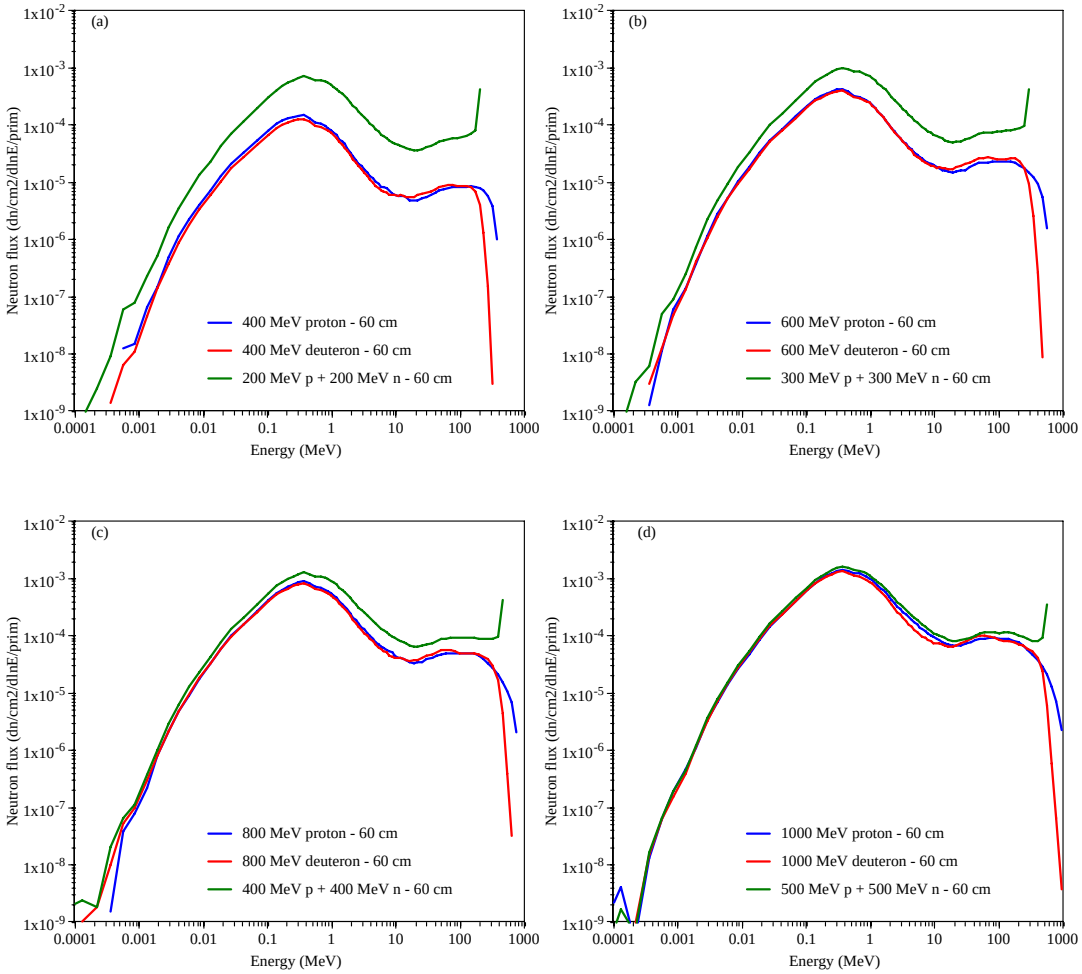

Figure 17. Neutron energy spectra for deuterons and protons at different target positions, for different energies.

Finally, the analysis of the power densities shows the difficulties of cooling a Multi-MW target driven by low energy deuterons since, for a σ ~1.7 mm Gaussian beam at 100 MeV, the power **densities** exceed 1 MW/cm^3/MW of beam, as illustrated in Figure 18.(a), where the power densities along the central axis are plotted, for several of deuteron energies. Notice that for energies above 400 MeV, the power density at the deuteron range lies well below the maximum value of the curve.

These maximum power densities significantly decrease with the incident particle energy, again an important argument to choose more energetic projectiles for high power spallation sources. Comparing protons and deuterons, the former present lower

power densities for all the energies analysed, from 35% lower at 400 MeV to 27% lower at 1 GeV, as indicated in Figure 18.(b).

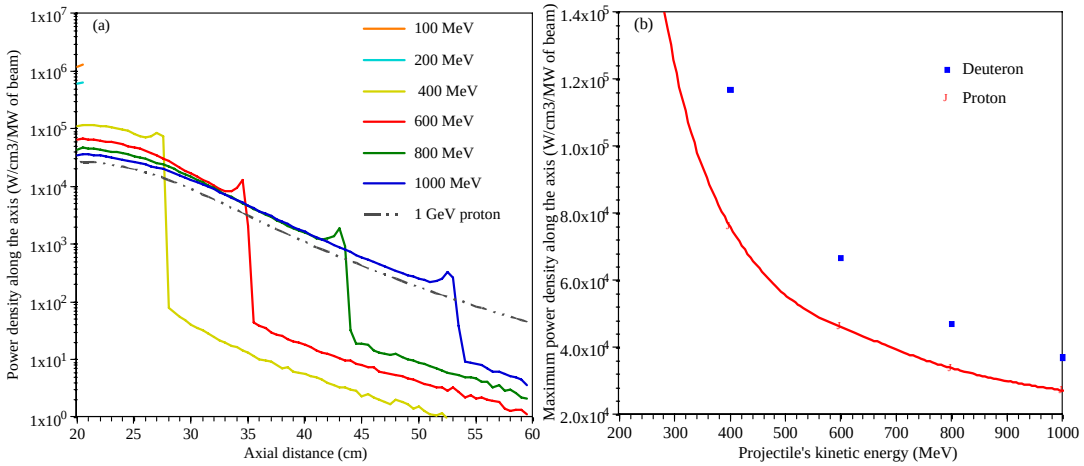

Figure 18. Energy deposition along the target axis for different incident particle energies (a), and the evolution of its maximum value (b).

Therefore, the choice of a short target driven by a low energy (few hundred MeV) high-intensity deuteron beam would present important difficulties in terms of heat removal, as well as operating in quite an inefficient energy range in terms of neutron yield (Figure 15.(b)). In addition, the limited gain in neutron flux through the use of deuterons at high projectile energies can hardly justifying the increase in technical complexity, thus higher costs, of a deuteron accelerator. Moreover, it would also worsen the already complex problem of removing the heat around the impact point in the liquid target.

Conclusions

An extensive set of calculations has been presented in this paper in order to define the basic parameters of the Multi-MW proton-to-neutron converter for the EURISOL project. The projectile nature and incident energy, target dimensions and materials and beam shape and, in general, the experimental layout have been discussed.

The use of a 1 or perhaps 2 GeV proton beam on a compact (~15 cm radius ~50 cm long) mercury target would bring about important neutron yields with a reasonable charged particle confinement. The increase in the proton energy up to 2 GeV and use of a wide Gaussian beam profile, or even better, an equivalent parabolic beam, significantly reduces the maximum power densities in the target. Improving the conditions for a proper heat removal, since this issue may be the bottleneck in the design.

For the fission target, natural uranium surrounded by a neutron reflector seems convenient option due to its availability and larger fission yields (potentially several times larger, for a moderated neutron spectrum) compared to depleted uranium. In fact, the low and intermediate energy fissions occurring in U-235 are **supplementary** to those occurring in U-238, which mostly take place at energies above 1 MeV.

Lead-bismuth eutectic as converter material may not be the optimum choice due to its greater technical complexity (heating required for such a liquid target due to its melting point at 125 °C and the production of important radiotoxic isotopes through irradiation), unless the maximum power densities cannot be maintained well below the melting point of mercury (~357 °C).

With respect to the use of deuterons as projectile, the neutron yield is increased in ~15% but the maximum power density is increased in ~30%. This fact and the increase in the costs of a deuteron machine would justify the choice of protons.

Considering these facts, a baseline design has been proposed, where a 15 cm radius 80 cm long mercury target with a conical void and a cylindrical flow guide has been designed, surrounded by a cooling helium tank. Around this converter block, a 3 cm thick UCx fission target has been foreseen, together with a beryllium oxide reflector to recuperate the escaping neutrons.

An extensive set of calculations has been performed on the aforementioned model, and will be presented in a following technical note. The initial results indicate that the required fission yields for the Multi-MW EURISOL target can be clearly achieved.

Acknowledgements

We acknowledge the financial support of the European Commission under the 6th Framework Programme “Research Infrastructure Action- Structuring the European Research Area” EURISOL DS Project Contract no. 515768 RIDS. The EC is not liable for any use that may be made of the information contained herein.

References

[1] *“EURISOL DS; European Isotope Separation On-Line Radioactive Ion Beam Facility Design Study”*, EC – FP6 Research Infrastructure Action- Structuring the European Research Area, Project Contract no. 515768 RIDS.

[2] *“FLUKA: Status and Prospective for Hadronic Applications”*, A. Fassò, A. Ferrari, J. Ranft, P.R. Sala, invited talk in the Proceedings of the MonteCarlo

2000 Conference, Lisbon, October 23--26 2000, A. Kling, F. Barao, M. Nakagawa, L. Tavora, P. Vaz eds., Springer-Verlag Berlin, p. 955-960, 2001. Also: *"Electron-photon transport in FLUKA: Status"*, A. Fassò, A. Ferrari, P.R. Sala, invited talk in the Proceedings of the MonteCarlo 2000 Conference, Lisbon, October 23--26 2000, A. Kling, F. Barao, M. Nakagawa, L. Tavora, P. Vaz eds., Springer-Verlag Berlin, p. 159-164, 2001.

[3] *"The EURISOL Report; A Feasibility Study for a European Isotope-Separation-On-Line Radioactive Ion Beam Facility"*, J. Cornell (Ed.), GANIL, France, 2003.

[4] *"Direct UCx Target for the SPES Project"*, A. Adrighetto, T3-01 Meeting, CERN, March 2005.

[5] *"European Spallation Source Technical Study"*, G. Bauer et al. (Eds.), ESS Council, 1997.

[6] Alberto Mengoni (IAEA, Vienna, Austria), private communication.